COMMUNICATIONS CHEMISTRY

ARTICLE

DOI: 10.1038/s42004-018-0061-8 OPEN

Light-regulated crystal growth of π-conjugated luminophores in an azobenzene matrix

Takuji Kobayashi[1], Yuichi Kitamoto[2], Yu Hirai[1], Takashi Kajitani[3,4], Tomohiro Seki[5] & Shiki Yagai[1,2]

Control over the phase transition of functional molecules is a key to design stimuli-responsive materials. Although many efforts have been devoted toward controlling the phase transition of functional molecules by various stimuli such as temperature, solvent vapor, and mechanical stimuli, indirect control using other stimuli-responsive molecules has been hardly explored. Here we demonstrate the potential of this methodology by using a luminescent and a photoresponsive molecule. We prepare blend films composed of an oligo(*p*-phenylenevinylene) amphiphile showing intrinsic luminescent chromism through isotropic-to-crystalline phase transition and a photo-liquefiable azobenzene amphiphile. The two materials are designed to co-assemble on the molecular level by introducing identical alkyl and oligo (ethylene glycol) chains. The blend films exhibit a luminescence color change from orange to green upon rubbing and subsequent exposure to UV light. Structural analyses reveal that the crystallization of the luminescent amphiphile is regulated by the photoinduced isotropization of the azobenzene amphiphile.

[1] Department of Applied Chemistry and Biotechnology, Graduate School of Engineering, Chiba University, 1-33 Yayoi-cho, Inage-ku, Chiba 263-8522, Japan. [2] Institute for Global Prominent Research (IGPR), Chiba University, 1-33 Yayoi-cho, Inage-ku, Chiba 263-8522, Japan. [3] Laboratory for Chemistry and Life Science, Institute of Innovative Research, Tokyo Institute of Technology, 4259 Nagatsuta, Midori-ku, Yokohama 226-8503, Japan. [4] RIKEN SPring-8 Center, 1-1-1 Kouto, Sayo, Hyogo 679-5148, Japan. [5] Division of Applied Chemistry & Frontier Chemistry Center, Faculty of Engineering, Hokkaido University, Sapporo, Hokkaido 060-8628, Japan. Correspondence and requests for materials should be addressed to S.Y. (email: yagai@faculty.chiba-u.jp)

Organic solid materials that exhibit tunable luminescent properties in response to external stimuli hold enormous promise for a range of applications in display, sensing, switching, and recording devices[1–12]. In many cases, luminescent properties change as a result of phase transitions, e.g., crystal-to-amorphous[13,14] or crystal-to-isotropic liquid transition[15,16], crystal-to-crystal transition[17–22], liquid crystal-to-crystal transition[23], and liquid crystal-to-liquid crystal transition[24], which can be triggered by various stimuli such as temperature, solvent vapor, and mechanical stimuli. Through these phase transitions, intermolecular interaction and/or the molecular conformation of luminogens alter, and these alterations are generally major origins of changes in luminescent properties. For all applications, precise stimulation in terms of resolution and switchability is of paramount importance, because it directly influences the performance of devices. As for such a "spatiotemporal controllability", none of the stimuli is superior to light[25,26]. So far, control over the luminescent property of organic molecules by light has been addressed only through an intricate molecular design that allows a compatible but interactive photochromic reaction and luminescence property in a single molecule[27–43]. In this context, indirect control over the phase transition of luminogens with other stimuli-responsive materials in a properly blended state can be proposed as an alternative approach and undoubtedly applied to many functional molecules; nevertheless this has been hardly addressed.

Herein, we demonstrate the potential of this approach by using a luminescent π-conjugated amphiphile and a photoresponsive azobenzene amphiphile. Self-assembly underpinned by molecular design enables the creation of functional organic materials with desired properties, which may be due to the high fidelity in controlling molecular arrangements on the atomic to nanoscopic level. This approach also enables co-assembly of two or more functional molecules in order to synergistically integrate their functional properties. Thus, we prepare blend films composed of an oligo(*p*-phenylenevinylene) amphiphile that shows a luminescent chromism from orange to green upon isotropic-to-crystalline phase transition, and an azobenzene amphiphile that shows a photoinduced liquid crystalline-to-isotropic phase transition. The two materials are designed to co-assemble on the molecular level, which is accomplished by using similar amphiphilic structures based on an identical hydrophobic alkyl chain and a hydrophilic oligo(ethylene glycol) chain. The blend films exhibit a luminescence color change from orange to green upon rubbing and exposing it subsequently to irradiation with UV light. Our structural analyses reveal that the crystallization of the luminescent amphiphile is regulated by the photoinduced isotropization of the azobenzene amphiphile.

Results

Molecular design. In a previous study, we have applied an amphiphilic molecular design to develop luminescent materials that respond to mechanical stimuli[44]. Amphiphile **1** (Fig. 1a), which bears a push–pull-type oligo(*p*-phenylenevinylene) luminophore, forms solution-processed aggregates that convert into metastable liquid crystals upon pressing, and further crystallize upon rubbing. This sequential phase transition is accompanied by a color change of the luminescence from yellow to orange and green. The yellow emission of the aggregates arises from π–π-stacked luminophores (π–π-stacked emission). In the present study, we focused on the orange→green color change of the luminescence that was observed for the liquid-crystal→crystal transition. In the liquid-crystalline state, the intramolecular charge-transfer (CT) emission (CT emission) with a large Stokes shift (~8500 cm^{-1}) is allowed for the dynamically twisting π-conjugated system, which is suppressed in the crystalline state on account of the diminished degrees of freedom of the π-conjugated system and the results in green emission (crystal emission). During further investigations on **1**, we discovered that the isotropic phase that resides above the liquid-crystalline phase (T_{iso} = 47 °C) can directly crystallize by crystal seeding at T_{iso} (Fig. 1b, c). Without crystal seeds, the isotropic phase is stable, and only a transition to the liquid-crystalline phase is observed upon cooling. We anticipated that this isotropic–crystalline phase transition might be controlled by light upon properly sequestering isotropic molecules of **1** in a photoswitchable molecular matrix (Fig. 1f, g).

For this purpose, we designed and synthesized azobenzene amphiphile **2**, which is based on the molecular structure of **1** (Fig. 1d). The molecular length of the benzyloxyazobenzene core in **2** is similar to that of the π-conjugated core of **1**, and hydrophobic dodecyl chains were introduced on the azobenzene side via the amino group, while a hydrophilic oligo(ethylene glycol) chain on the benzyloxy side was incorporated via the ester group. We expected that the comparable molecular lengths and amphiphilic structures of **1** and **2** might suppress their macroscopic phase separation.

Phase-transition behavior of azobenzene amphiphile. Polarized optical microscopy (POM) and differential scanning calorimetry (DSC) analyses showed that films of **2** that are cast from acetonitrile solution form a monotropic liquid crystal between 24 and 36 °C upon heating (Supplementary Figures 1and 2). A powder X-ray diffraction (PXRD) analysis revealed a bilayer structure for the mesophase with an inter-bilayer spacing of 57.0 Å (Supplementary Figure 3a). When the mesophase of **2** was irradiated with UV light ($\lambda = 365$ nm), a reversible isotropization was confirmed by POM, optical microscopy (OM), and a PXRD analysis (Fig. 1e, f and Supplementary Figure 3b). This UV-induced isotropic phase was fluidal, suggesting that it was an isotropic liquid. While only a minuscule absorption change was observed upon irradiation with UV light (Supplementary Figure 4), clear spectral changes reflecting the photoisomerization were observed by absorption and ^{1}H NMR spectroscopy when **2** was dissolved in THF (Supplementary Figure 5). This is most likely due to a *trans*-to-*cis* UV-induced photoisomerization followed by a rapid *cis*-to-*trans* thermal isomerization, given the thermal instability of the *cis*-isomer; this mutual *trans–cis* isomerization should be responsible for the photoinduced isotropization of **2**[45–47].

Phase-transition behavior of a blend film. Figure 2a displays the stimuli-responsive photoluminescent color change of a blend film of **1** and **2** under weak irradiation with UV light. The blend film was prepared by casting an acetonitrile solution of an equimolar mixture of **1** and **2**. The as-prepared film exhibited red/orange color under irradiation with UV light. Fluorescence spectroscopy measurements showed an emission band at 587 nm, which is consistent with the CT emission from **1** [44]. Upon rubbing the as-prepared film, we obtained a waxy film that exhibited orange photoluminescence with an emission maximum at 605 nm (Figs. 2a, b). The bathochromic shift of 18 nm by rubbing might be more homogeneous mixing of **1** within the liquid-crystalline matrix of **2**, which could cause stabilization of charge-transfer excited state of **1**. Henceforth, we will refer to this film as the **O** film. When the **O** film was irradiated with UV light (LED lamp, $\lambda = 365$ nm), the luminescence color gradually changed from orange to green (Fig. 2a). The time-course fluorescence analysis using a microscopic spectral apparatus ($\phi = 0.1$ mm) revealed that the CT emission of **1** gradually decreased upon UV irradiation, which was compensated by the growth of a structured emission with a maximum at 540 nm and a shoulder at 498 nm

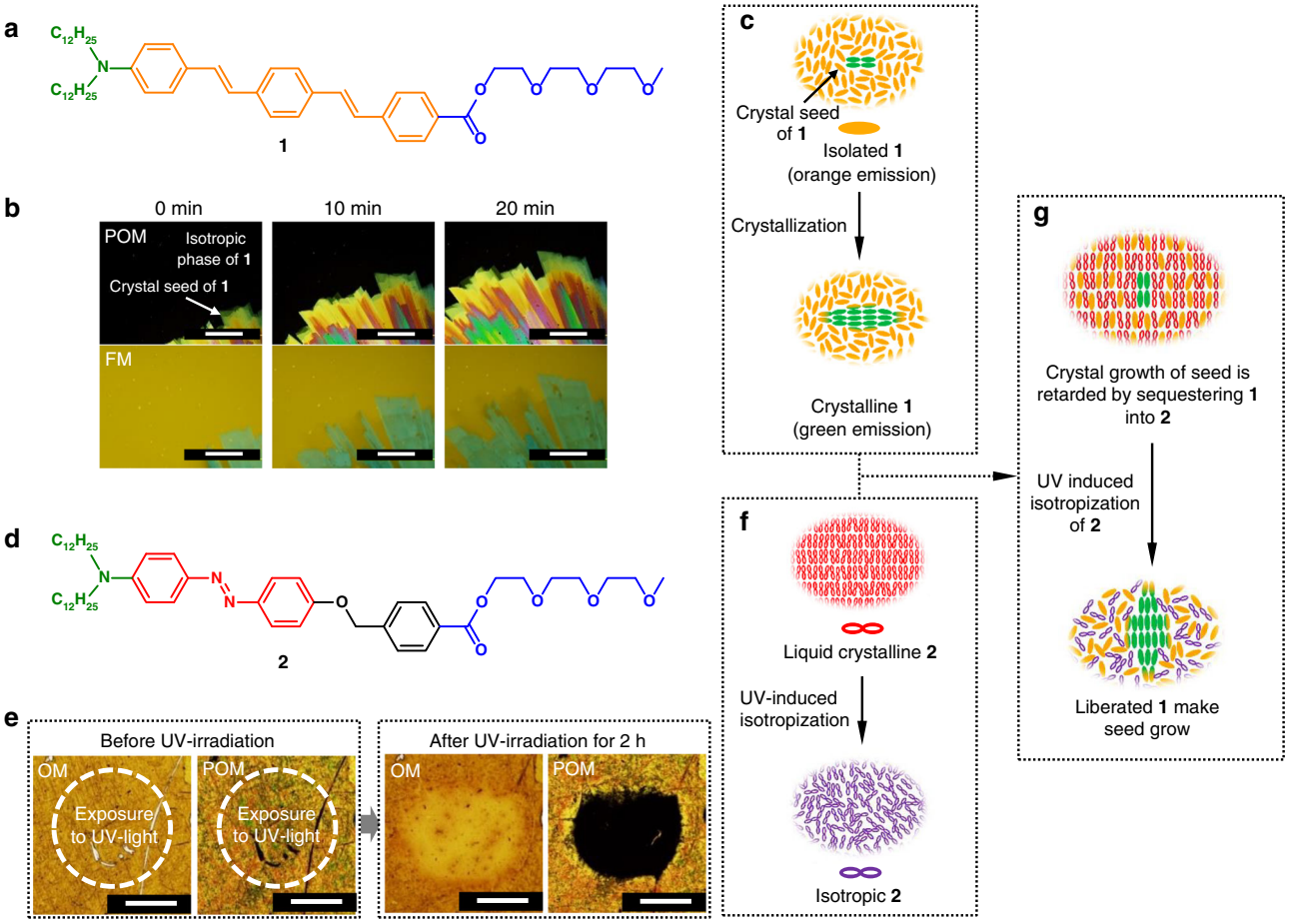

Fig. 1 The concept of light-regulated crystal growth. **a**, **d** Chemical structures of the amphiphilic oligo(*p*-phenylenevinylene) luminophore **1** and the amphiphilic azobenzene photoswitch **2**. **b** Polarized optical microscopy (POM) images and fluorescence microscopy (FM) images for the seeded crystal growth of **1** from the isotropic liquid phase at 50 °C. Scale bars: 100 μm. **c** Schematic illustration of the crystallization of **1** from the isotropic phase. **e** POM and optical microscopy (OM) images for the UV-induced isotropization of liquid-crystalline **2** at 28 °C. Scale bars: 300 μm. **f** Schematic illustration of the UV-induced isotropization of **2**. **g** Schematic illustration of the UV-induced crystallization of **1** blended with **2**

(Fig. 2c), which is similar to that of the crystal emission of **1**. After 30 min of UV irradiation, the luminescence color of the film had changed from orange to green. The degree of this emission color change was dependent on the intensity of UV light (Supplementary Figure 6). These observations suggest that UV irradiation of the **O** film induces the crystallization of **1**, even though it does not respond to UV light itself. The thermal effect of the LED light source, which could also accelerate the crystal growth of **1**, was excluded based on a thermographic analysis (Supplementary Figure 7). Henceforth, we will refer to this UV-induced green-emitting film as the **G** film. It is worth noting that the conversion of the as-prepared film to the **G** film requires both (i) rubbing and (ii) UV irradiation in this order; if the as-prepared film was exposed to UV irradiation prior to rubbing, a luminescence color change was not observed.

Mechanism of phase transition. The mechanism of this stimuli-responsive luminescence color change was investigated by PXRD analysis and DSC. The PXRD pattern of the solution-cast film involves two sets of diffractions that can be assigned to lamellar structures with interlayer spacings of $d = 57.0$ Å and $d = 42.7$ Å (Fig. 3a). The former, stronger diffraction set can be attributed to the liquid crystals of **2**, whereas the latter, weaker diffraction set arises from the π–π-stacked aggregates of **1**[44]. Accordingly, upon solution-casting the mixture of **1** and **2**, a part of **1** forms phase-separated π–π-stacked aggregates, while the remaining part might be mixed with liquid crystals of **2** in a molecularly dispersed state that shows CT emission. In the DSC trace of the as-prepared film, only a single endothermic peak was observed at 31 °C ($\Delta H = 5.4$ kcal mol^{-1}), which was attributed to the isotropization of liquid-crystalline **2** (Fig. 3b). The phase-transition peaks of aggregated **1** to the liquid-crystalline phase (37 °C) and subsequently to the isotropic phase (47 °C) were not observed.[44] This suggests that above 31 °C, aggregates of **1** can be molecularly dissolved in the isotropic liquid pool of **2**. This was further confirmed by the PXRD pattern measured at 36 °C, wherein the diffraction of the aggregates of **1** disappeared completely (Supplementary Figure 8).

When the solution-cast film was converted into the **O** film by rubbing, the diffraction set of liquid-crystalline **2** remained unchanged, whereas that of aggregated **1** was replaced with an intense lamellar diffraction set with an interlayer spacing of d=39.1 Å (Fig. 3a). This new diffraction set is consistent with that of crystalline **1**, which suggests that the mechanical stimulation of the as-prepared film produces crystalline domains of **1** in the liquid-crystalline matrix of **2**, which can subsequently act as seeds for further crystal growth[44]. However, continuous rubbing of the **O** film did not induce the transformation into the **G** film. Accordingly, the mechanical stimulation does not induce spontaneous crystallization of the molecularly dispersed **1** with

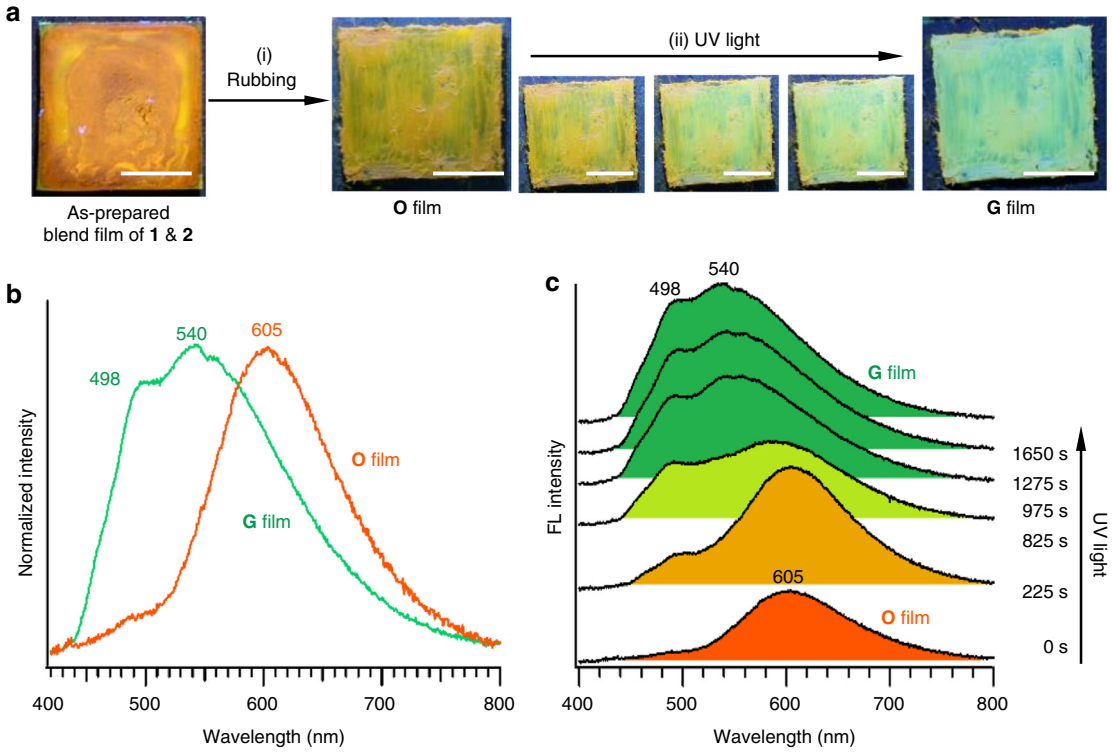

Fig. 2 UV-induced luminescence color change. **a** Fluorescence images that show the photo-induced luminescence color change of the as-prepared blend film of **1** and **2**, recorded under irradiation with weak UV light. Orange-emitting **O** films can be converted into green-emitting **G** films by irradiation with UV light using an LED lamp (17 mW/cm^2, $\lambda = 365$ nm) for 1 h. Scale bars: 0.5 cm. **b** Fluorescence spectra ($\lambda_{ex} = 365$ nm) of **O** film, and **G** film. **c** Time-course fluorescence spectral change of the **O** film upon exposure to UV irradiation

liquid crystals of **2** but does transform the aggregated domains of **1** into crystalline seeds (Fig. 3c).

The formation of a crystalline seed of **1** by rubbing was supported by the DSC trace of the **O** film, wherein a small endothermic peak was observed at 42 °C ($\Delta H = 0.42$ kcal mol^{-1}) after the isotropization of liquid-crystalline **2** at 31 °C (Fig. 3b). As the pure crystalline **1** shows the isotropization transition at 54 °C[44], the transition peak at 42 °C can be attributed to the dissolution of crystal seeds of **1** in the isotropic liquid of **2**. This was also confirmed by a dissolution experiment of separately prepared crystals of **1** in the isotropic phase of **2** at 43 °C (Supplementary Figure 10). Despite the formation of crystal seeds of **1**, the fluorescence of the **O** film is governed by the orange CT emission of molecularly dissolved **1** as has already been shown in Fig. 2b. It is therefore most likely that the majority of the molecules of **1** are dispersed and sequestered within the liquid-crystalline matrix of **2** in the **O** film (Fig. 3c), which provides a reasonable explanation for why crystal seeds of **1** cannot grow spontaneously in the **O** film.

The PXRD pattern of the **G** film showed only diffractions arising from crystalline **1**, which suggests a selective photo-induced isotropization of **2** (Fig. 3a). This result is corroborated by the disappearance of the isotropization peak of liquid-crystalline **2** at 31 °C in the DSC trace of the **G** film (Fig. 3b). Importantly, the transition enthalpy ($\Delta H = 4.0$ kcal mol^{-1}) of the melting transition of crystalline **1** into the liquid-crystalline matrix of **2** in the **G** film is by one order of magnitude higher than that of the **O** film ($\Delta H = 0.42$ kcal mol^{-1}). Grazing-incidence wide-angle X-ray diffraction (GI-WAXD) measurements revealed a 1.8-fold increase in diffraction intensity of crystalline **1** after the **O**→**G** conversion (Supplementary Figure 11). These results corroborate that the photoinduced isotropization of **2** can induce the crystal growth of **1**. Namely, molecules of **1** sequestered in the liquid-crystalline matrix of **2** can be liberated upon UV-induced isotropization of **2**, and the increased mobility of **1** in the isotropic liquid matrix of **2** thus accelerates the crystal growth (Fig. 3c). Reflecting this mechanism, heating the **O** film above 31 °C (above the m.p. of **2**) but below 42 °C (below the m.p. of **1** in the liquid matrix of **2**) caused the **O**→**G** conversion without UV irradiation (Supplementary Figure 9).

To shed further light on the photoinduced crystal growth, POM measurements were carried out for the **O**→**G** conversion. In Fig. 3d, the top four panels show a time-course change (15 min) of POM images of crystalline seeds of **1** in the **O** film just after preparation. The birefringent crystalline domains of **1** propagate very slowly (30 μm/h) in the less birefringent liquid-crystalline matrix of **2** that includes molecularly dispersed **1**. On the other hand, the bottom four panels show the subsequent time-course change under irradiation with UV light. The crystal growth is accelerated by a factor of 4 (120 μm/h) under UV light, and after 15 min, the observation area was mostly covered by crystalline domains of **1**.

Reversibility. We also explored the reversibility of the photo-generated **G** film into the **O** film by mechanical stimuli. Upon rubbing the **G** film, the luminescence color reverted to orange, albeit to a slightly greenish orange (Fig. 4a), which was spectroscopically reflected in a broad emission from 450 to 700 nm (Fig. 4b). In this context, we should thus discriminate this second orange-emitting film (**O′** film) from the original **O** film that was prepared from casting a solution. In fact, a DSC analysis of the **O′** film showed $\Delta H = 4.2$ kcal mol^{-1} for the transition at 42 °C, which is comparable to that of the **G** film. This **G**→**O′** conversion

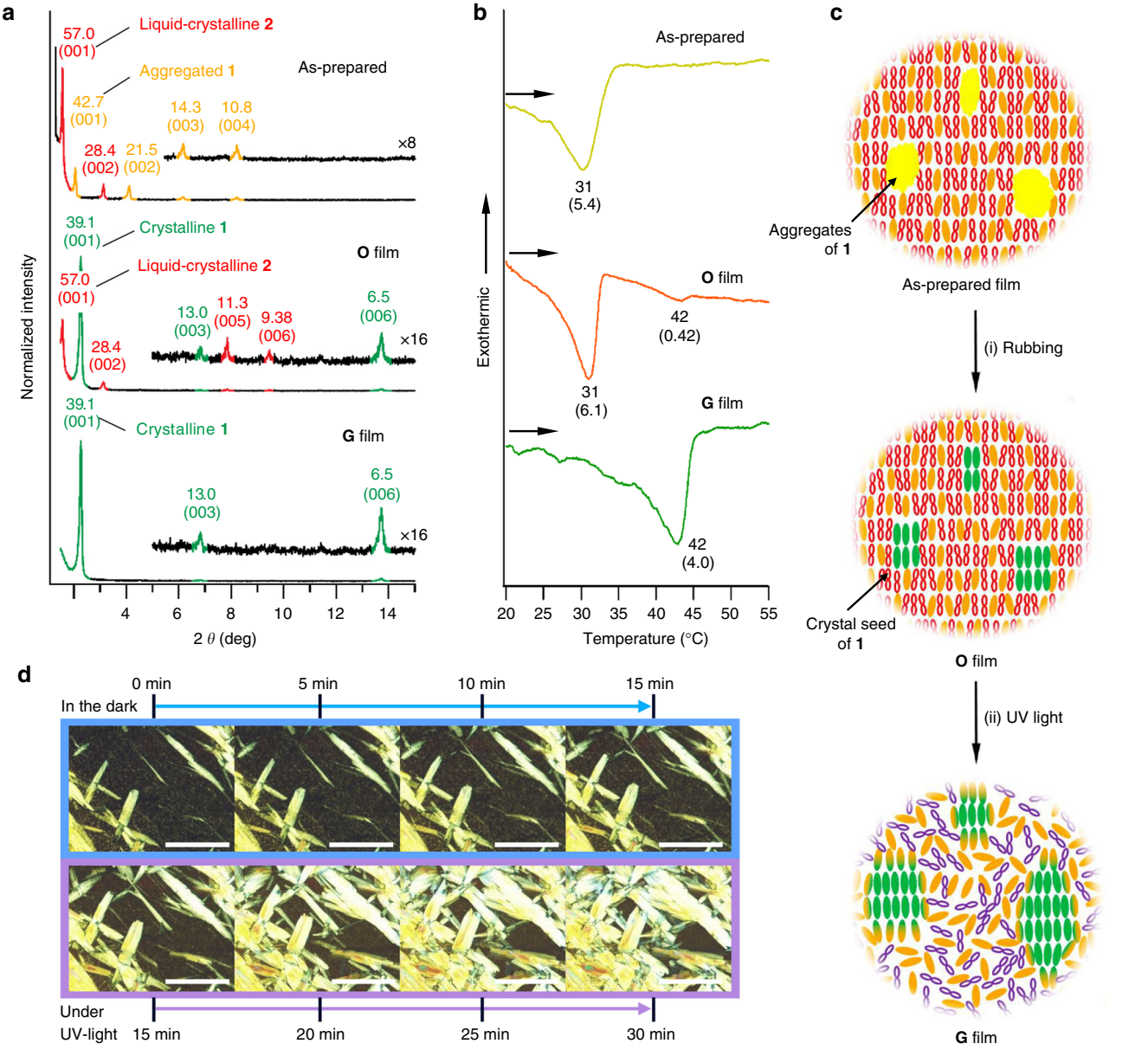

Fig. 3 Analysis and mechanism of the UV-induced crystal growth. **a** PXRD patterns of the as-prepared film, **O** film, and **G** film of **1** and **2** at 25 °C with major *d*-spacings in Å (Miller indices in parenthesis). **b** DSC thermograms (temperature gradient: 1 °C min^{-1}) of the as-prepared film, **O** film, and **G** film of **1** and **2**. The temperatures for the phase-transition peaks are shown in °C with associated enthalpy changes (in kcal mol^{-1}) in brackets. All the samples were separately prepared on different glass plates and transferred to DSC pans. **c** Schematic illustration of the mechanism of the mechano- and photo-induced phase transitions. **d** Time-course POM images of the crystal growth of **1** in the **O** film in the dark and under irradiation with UV light at 25 °C. Scale bars: 100 μm

is thus probably caused by the mechanical fragmentation and possible dissolution of crystallized **1** in the isotropic liquid-crystalline matrix of **2**. The **O′** film could be converted into a green-emitting film (**G′** film) by exposure to UV light (Fig. 4a). The emission spectrum of the **G′** film is sharper than that of the **G** film due to decreased contamination from the CT emission arising from molecularly dispersed **1** (Fig. 4b).

The difference between the **G** and **G′** films was more clearly demonstrated by a photo-patterning experiment involving a sequential **O**→**G**→**O′**→**G′** conversion and a photomask (Fig. 4c–g). For the **O**→**G** and **O′**→**G′** conversions, the identical UV irradiation conditions were applied. While crystalline grains of **1** can be clearly seen in the POM image of the **G** film (Fig. 4h, i), no such crystalline grains were observed for the **G′** film (Fig. 4j, k). As a result, the **G′** film shows much better photo-patterned images with a resolution below 50 μm (Fig. 4k). As the crystal seeds of **1** in the **O** film are provided by a mechanical conversion of the aggregated **1**, their formation should be limited. As a result, they can be fed with a large amount of molecularly dispersed **1** through the photo-isotropization of **2**, and thus grow into larger crystals to give the **G** film (Fig. 4h, i). At the same time, the limited formation of crystal seeds should hamper the complete consumption of photo-liberated molecules of **1**, which would result in a crystalline emission that is contaminated with the CT emission in the **G** film. In contrast, the crystal seeds in the **O'** film are provided by mechanically crushing such large crystals of **1** in

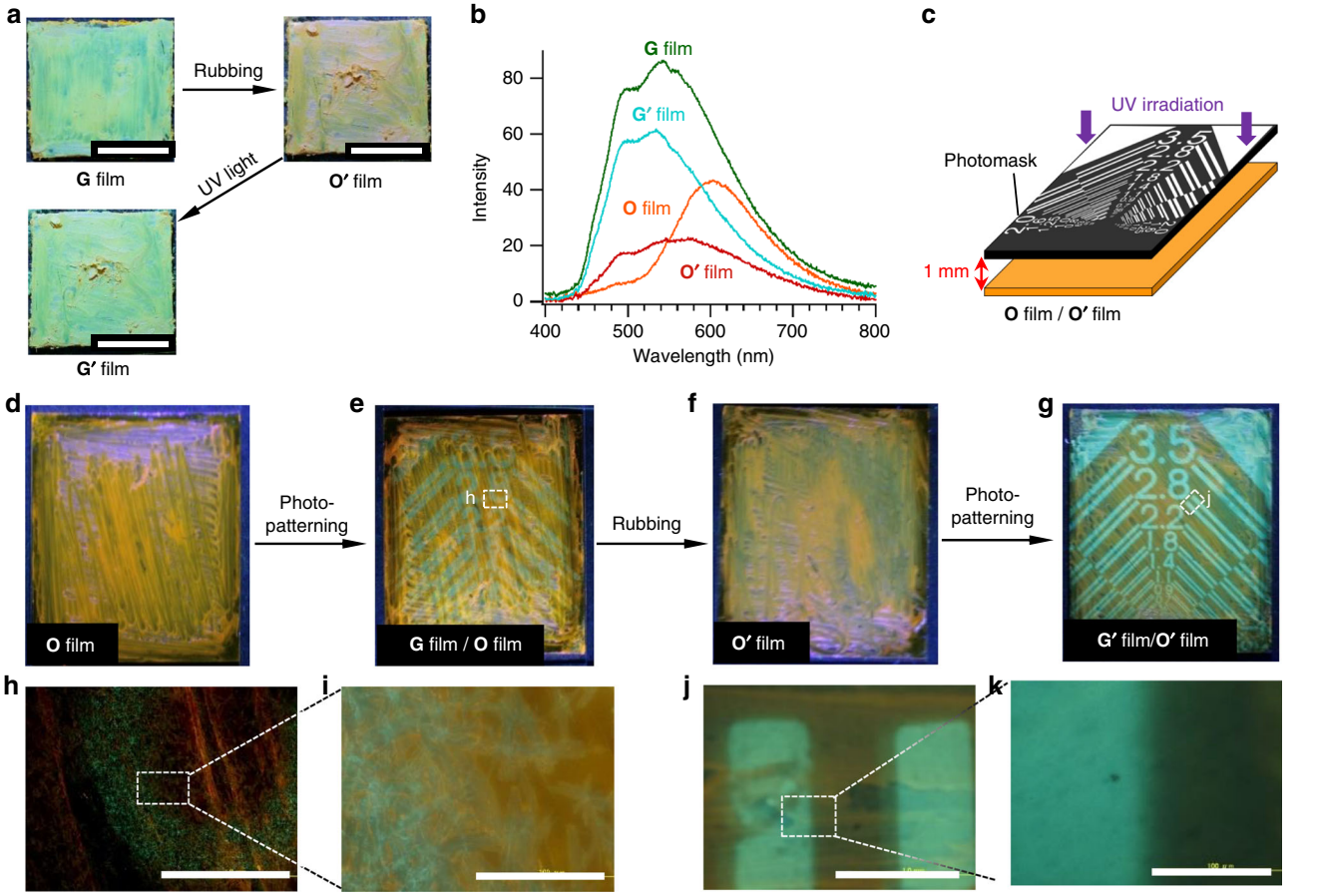

Fig. 4 Reversibility of the luminescence color change and photo-patterning experiment. **a** Fluorescence images for the sequential **G**→**O**′→**G**′ conversion. Scale bars: 0.5 cm. **b** Fluorescence spectral change for the **O**→**G**→**O**′→**G**′ conversion. **c** Schematic representation of a photo-patterning experiment for the **O**→**G** and **O**′→**G**′ conversions. **d**–**g** Fluorescence images for the sequential **O**→**G**→**O**′→**G**′ conversion using the photomask shown in (**c**). **h**, **j** Fluorescence micrographs of a part of (**e**) and (**g**), respectively. Scale bars: 1 mm. **i**, **k** Fluorescence micrographs of a part of (**h**) and (**j**), respectively. Scale bars: 100 μm

the **G** film. As a result, the photoinduced crystalline growth may be initiated by a large amount of the resulting fine crystals, which would enable high-resolution photo-patterning as well as more efficient consumption of the photo-liberated molecules of **1**.

Discussion

In conclusion, we have presented a rational self-assembly strategy to impart a mechanochromic luminescent material with photo-responsive properties. A key to realizing this strategy is sequestering a crystallizable luminescent chromophore within a liquid-crystalline matrix of a photoswitchable molecule through amphiphilic co-assembly. This specific ensemble of two functional molecules can realize the light-induced liberation of the sequestered luminophores through a phase transition of the photoswitchable molecules. Although we have applied an amphiphilic molecular design in this study to develop the aforementioned molecular ensemble, we may be able to employ a wider variety of supramolecular assembly strategies to integrate two or more molecules of orthogonal functionality in the bulk.

Methods

General information. Solid-state UV/Vis absorption spectra were recorded on a JASCO V660 spectrophotometer. Fluorescence spectra were recorded on a JASCO FP6600 spectrofluorometer and a Hitachi F-7000 spectrometer. Fluorescence microscopic spectra of the blend film were recorded on a photonic multichannel analyzer (Hamamatsu Photonics). ^{1}H and ^{13}C NMR spectra were recorded on JEOL JNM-ECA500 spectrometer and chemical shifts are reported in ppm (δ) with the signal of TMS as internal standard. ESI-HRMS was measured on a Exactive (Thermo Scientific).

Materials. Compound **2** was synthesized according to the method reported in the Supplementary Methods and characterized by ^{1}H and ^{1}C NMR (Supplementary Figures 12 and 13, respectively) and ESI-MS spectrometry. Column chromatography was performed using 63–210-μm silica gel. All other commercially available reagents and solvents were reagent grade and used without further purification. The solvents for the spectroscopic measurements were all spectral grade and used without further purification.

Film preparation. All film samples were prepared on a glass substrate except for those for GI-XRD analysis, which were prepared on a silicon substrate. The blend film was prepared by drying an equimolar mixture of **1** (2.4 mM) and **2** (2.4 mM) in acetonitrile on a grass substrate. The resulting film was converted to the **O** film by rubbing using a spatula.

Photoirradiation experiments. Photoirradiation experiments were performed using a UV LED lamp ($\lambda = 365$ nm) with an intensity of 17 mW/cm^2 (at a distance of 5 cm). The distance between the light source and the samples was 5 cm. With this condition, the diameter of the light spot on the sample is ca. 5 cm, which completely covers the whole area of the samples (1.2 × 1.2 cm^2).

Differential scanning calorimetry measurements. DSC was performed on SII DSC6220. For the DSC analysis of the mixtures of **1** and **2**, we first separately prepared the as-prepared, **O** and **G** films on glass plates. Then we scraped the film by a spatula and transferred it to DSC pans.

Polarized optical microscopy. Polarized optical microscopic observation was carried out using an Olympus BX51 optical microscopy system with a Linkam temperature-controlled heating stage.

Powder X-ray diffraction analysis. PXRD analysis was carried out with a Rigaku Rint-2200 X-ray diffractometer with monochromated CuKα ($\lambda = 1.54$ Å) radiation and temperature-controlled heating stage.

Grazing-incidence X-ray diffraction analysis. X-ray diffraction experiments were carried out on the BL45XU beamline at SPring-8 (Hyogo, Japan) using a Pilatus3X 2M (Dectris) detector. The scattering vector ($q = 4\pi\sin\theta/\lambda$) and the position of the incident X-ray beam on the detector were calibrated using several orders of layer reflections from silver behenate ($d = 58.380$ Å), where 2θ and λ refer to the scattering angle and wavelength of the X-ray beam (1.00 Å), respectively. The sample-to-detector distance was 0.30 m.

Data availability

All relevant data supporting the findings of this study are available within the article and its Supporting information files, and from the corresponding author upon reasonable request.

Received: 22 August 2018 Accepted: 6 September 2018
Published online: 26 September 2018

References

1. Yan, D. & Evans, D. G. Molecular crystalline materials with tunable luminescent properties: from polymorphs to multi-component solids. *Mater. Horiz.* **1**, 46–57 (2014).
2. Wenger, O. S. Vapochromism in organometallic and coordination complexes: chemical sensors for volatile organic compounds. *Chem. Rev.* **113**, 3686–3733 (2013).
3. Sagara, Y. & Kato, T. Mechanically induced luminescence changes in molecular assemblies. *Nat. Chem.* **1**, 605–610 (2009).
4. Lustig, W. P. et al. Metal–organic frameworks: functional luminescent and photonic materials for sensing applications. *Chem. Soc. Rev.* **46**, 3242–3285 (2017).
5. Cui, Y., Chen, B. & Qian, G. Lanthanide metal-organic frameworks for luminescent sensing and light-emitting applications. *Coord. Chem. Rev.* **273–274**, 76–86 (2014).
6. Thomas, S. W. III, Joly, G. D. & Swager, T. M. Chemical sensors based on amplifying fluorescent conjugated polymers. *Chem. Rev.* **107**, 1339–1386 (2007).
7. Yan, X., Wang, F., Zheng, B. & Huang, F. Stimuli-responsive supramolecular polymeric materials. *Chem. Soc. Rev.* **41**, 6042–6065 (2012).
8. Wang, X.-d, Wolfbeis, O. S. & Meier, R. J. Luminescent probes and sensors for temperature. *Chem. Soc. Rev.* **42**, 7834–7869 (2013).
9. Babu, S. S., Praveen, V. K. & Ajayaghosh, A. Functional π-gelators and their applications. *Chem. Rev.* **114**, 1973–2129 (2014).
10. Liu, G. & Zhao, Y. L. Switching between phosphorescence and fluorescence controlled by chiral self-assembly. *Adv. Sci.* **4**, 1700021 (2017).
11. Seki, T. & Ito, H. Molecular-level understanding of structural changes of organic crystals induced by macroscopic mechanical stimulation. *Chem. Eur. J.* **22**, 4322–4329 (2016).
12. Sagara, Y., Yamane, S., Mitani, M., Weder, C. & Kato, T. Mechanoresponsive luminescent molecular assemblies: an emerging class of materials. *Adv. Mater.* **28**, 1073–1095 (2016).
13. Fernández-Mato, A. et al. Polymorphism-triggered reversible thermochromic fluorescence of a simple 1,8-naphthyridine. *Cryst. Growth Des.* **13**, 460–464 (2013).
14. Ito, H. et al. Reversible mechanochromic luminescence of $[(C_6F_5Au)_2(\mu$-1,4-diisocyanobenzene)]. *J. Am. Chem. Soc.* **130**, 10044–10045 (2008).
15. Yagai, S. et al. Mechanochromic luminescence based on crystal-to-crystal transformation mediated by a transient amorphous state. *Chem. Mater.* **28**, 234–241 (2016).
16. Yoon, S. J. & Park, S. Y. Polymorphic and mechanochromic luminescence modulation in the highly emissive dicyanodistyrylbenzene crystal: secondary bonding interaction in molecular stacking assembly. *J. Mater. Chem.* **21**, 8338–8346 (2011).
17. Kong, Q. et al. High contrast stimuli-responsive luminescence switching of pyrene-1-carboxylic esters triggered by a crystal-to-crystal transition. *New J. Chem.* **41**, 13784–13791 (2017).
18. Zhao, Y. et al. Thermally induced reversible phase transformations accompanied by emission switching between different colors of two aromatic-amine compounds. *Adv. Mater.* **21**, 3165–3169 (2009).
19. Lim, S. H., Olmstead, M. M. & Balch, A. L. Molecular accordion: vapoluminescence and molecular flexibility in the orange and green luminescent crystals of the dimer, $Au_2(\mu$-bis-(diphenylphosphino)ethane$)_2Br_2$. *J. Am. Chem. Soc.* **133**, 10229–10238 (2011).
20. Ito, H. et al. Mechanical stimulation and solid seeding trigger single-crystal-to-single-crystal molecular domino transformations. *Nat. Commun.* **4**, 2009 (2013).
21. Seki, T., Sakurada, K., Muromoto, M. & Ito, H. Photoinduced single-crystal-to-single-crystal phase transition and photosalient effect of a gold(I) isocyanide complex with shortening of intermolecular aurophilic bonds. *Chem. Sci.* **6**, 1491–1497 (2015).
22. Yoon, S.-J. et al. Multistimuli two-color luminescence switching via different slip-stacking of highly fluorescent molecular sheets. *J. Am. Chem. Soc.* **132**, 13675–13683 (2010).
23. Han, K. & Cho, B. K. Monoclinic to two-dimensional hexagonal transformation in hexacatenar molecules with a 1,2,3-triazole-based conjugated rod: morphology-dependent thermochromic behavior. *Soft Matter* **10**, 7588–7594 (2014).
24. Sagara, Y. & Kato, T. Brightly tricolored mechanochromic luminescence from a single-luminophore liquid crystal: reversible writing and erasing of images. *Angew. Chem. Int. Ed.* **50**, 9128–9132 (2011).
25. Yagai, S., Karatsu, T. & Kitamura, A. Photocontrollable self-assembly. *Chem. Eur. J.* **11**, 4054–4063 (2005).
26. Yagai, S. & Kitamura, A. Recent advances in photoresponsive supramolecular self-assemblies. *Chem. Soc. Rev.* **37**, 1520–1529 (2008).
27. Han, M. & Hara, M. Intense fluorescence from light-driven self-assembled aggregates of nonionic azobenzene derivative. *J. Am. Chem. Soc.* **127**, 10951–10955 (2005).
28. Zhu, L. et al. Unimolecular photoconversion of multicolor luminescence on hierarchical self-assemblies. *J. Am. Chem. Soc.* **135**, 5175–5182 (2013).
29. Seo, J., Chung, J. W., Kwon, J. E. & Park, S. Y. Photoisomerization-induced gel-to-sol transition and concomitant fluorescence switching in a transparent supramolecular gel of a cyanostilbene derivative. *Chem. Sci.* **5**, 4845–4850 (2014).
30. Wei, P. et al. Multiple yet controllable photoswitching in a single AIEgen system. *J. Am. Chem. Soc.* **140**, 1966–1975 (2018).
31. Irie, M., Fukaminato, T., Sasaki, T., Tamai, N. & Kawai, T. A digital fluorescent molecular photoswitch. *Nature* **420**, 759–760 (2002).
32. Fukaminato, T. & Irie, M. Reversible fluorescence wavelength shift based on photoinduced aggregate formation. *Adv. Mater.* **18**, 3225–3228 (2006).
33. Berberich, M., Krause, A.-M., Orlandi, M., Scandola, F. & Würthner, F. Toward fluorescent memories with nondestructive readout: photoswitching of fluorescence by intramolecular electron transfer in a diaryl ethene-perylene bisimide photochromic system. *Angew. Chem. Int. Ed.* **47**, 6616–6619 (2008).
34. Fukaminato, T. et al. Single-molecule fluorescence photoswitching of a diarylethene-perylenebisimide dyad: non-destructive fluorescence readout. *J. Am. Chem. Soc.* **133**, 4984–4990 (2011).
35. Yagai, S. et al. Rational design of photoresponsive supramolecular assemblies based on diarylethene. *Chem. Eur. J.* **19**, 6971–6975 (2013).
36. Yagai, S. et al. Photocontrol over self-assembled nanostructures of π–π stacked dyes supported by the parallel conformer of diarylethene. *Angew. Chem. Int. Ed.* **53**, 2602–2606 (2014).
37. Bu, J., Watanabe, K., Hayasaka, H. & Akagi, K. Photochemically colour-tuneable white fluorescence illuminants consisting of conjugated polymer nanospheres. *Nat. Commun.* **5**, 3799 (2014).
38. Park, S. K. et al. Stimuli-responsive reversible fluorescence switching in a crystalline donor–acceptor mixture film: mixed stack charge-transfer emission versus segregated stack monomer emission. *Angew. Chem. Int. Ed.* **55**, 203–207 (2016).
39. Kitagawa, D. et al. Polymorphs of a diarylethene that exhibits strong emission and direct visualization of polymorphic phase transition process by fluorescence color change. *Dyes Pigments* **139**, 233–238 (2017).
40. Kashihara, R., Morimoto, M., Ito, S., Miyasaka, H. & Irie, M. Fluorescence photoswitching of a diarylethene by irradiation with single-wavelength visible light. *J. Am. Chem. Soc.* **139**, 16498–16501 (2017).
41. Qi, Q. et al. Solid-state photoinduced luminescence switch for advanced anticounterfeiting and super-resolution imaging applications. *J. Am. Chem. Soc.* **139**, 16036–16039 (2017).
42. Wang, J. et al. Organoboron-based photochromic copolymers for erasable writing and patterning. *Macromolecules* **50**, 4629–4638 (2017).
43. Genovese, D. et al. Mechano- and photochromism from bulk to nanoscale: data storage on individual self-assembled ribbons. *Adv. Funct. Mater.* **26**, 5271–5278 (2016).
44. Yagai, S. et al. Design amphiphilic dipolar π-systems for stimuli-responsive luminescent materials using metastable states. *Nat. Commun.* **5**, 4013 (2014).
45. Ikeda, T. & Tsutsumi, O. Optical switching and image storage by means of azobenzene liquid-crystal films. *Science* **268**, 1873–1875 (1995).

46. Bandarab, H. M. D. & Burdette, S. C. Photoisomerization in different classes of azobenzene. *Chem. Soc. Rev.* **41**, 1809–1825 (2012).
47. Seki, T. A wide array of photoinduced motions in molecular and macromolecular assemblies at interfaces. *Bull. Chem. Soc. Jpn.* **91**, 1026–1057 (2018).

Acknowledgements

This work was supported by JSPS KAKENHI Grant Numbers JP15H03855 and 26102010; a Grant-in-Aid for Scientific Research on Innovative Areas "π-Figuration" (26102001). S.Y. thanks Konika Minolta Science and Technology Foundation for partial financial support. The synchrotron XRD experiments were performed at the BL45XU in the SPring-8 with the approval of the RIKEN SPring-8 Center (proposal number 20170055).

Author contributions

S.Y. and T.Ko. conceptualized the project. T.Ko. has performed most of the experiments described in the manuscript including the synthesis of the molecule **2**. Y.K., Y.H., and T.S. helped some experimental procedures and discussed on the results. T.Ka. collected GI-WAXD data and discussed the mechanism. T.Ko. and S.Y. wrote the overall manuscript and worked on the figures. All authors commented on the manuscript.

Additional information

Supplementary information accompanies this paper at https://doi.org/10.1038/s42004-018-0061-8.

Competing interests: The authors declare no competing interests.